4

Final Report for

A Study of the Relationship Between Macroscopic Measures and Physical Processes Occurring During Crack Closure

N0014-89-J-1708

Submitted to:

Office of Naval Research
Attn. Dr. George Yoder
ONR Code 1131
800 N. Quincy
Arlington, Virginia 22217-5000

by

Stuart R. Stock
Mechanical Properties Res. Lab
School of Materials Sci. & Eng.
Georgia Institute of Technology
Atlanta, Ga 30332-0245

Stephen D. Antolovich
Dept. of Mechanical & Mat. Eng.
Washington State University
Pullman, WA 99164-2920

Table of Contents

Abstract

This report is divided into Parts A and B which cover the numerical modeling with supporting fractography and the high resolution x-ray computed tomography of loaded samples, respectively. The figures for each part immediately follow the text of that part. The focus throughout is to relate macroscopic measures of crack closure to the physical processes occurring at and near the crack tip.

The most significant accomplishments of the program detailed in Part A include the following. Roughness-induced crack closure was characterized by fractographic analysis. The crack tip stress parameter, K, was justified as a forcing function at the crack tip in the roughness-induced crack closure problem. Analytical models were developed to predict the closure stress intensity factor as a function of crack length using a "phenomenological approach." The relations between fractographically measured parameters and the crack driving "force" was investigated.

In Part B, results of high resolution x-ray computed tomography of loaded notched tensile and compact tension samples are discussed. The use of a miniature load frame, developed as part of this project, allowed measurements of crack opening across the entire crack face to be made as a function of applied load. Discussion of these nondestructive measurements is included.

Part A. I. Introduction

In all computational work to date, crack closure was simulated through calculation of effective stress intensity factors. The situation addressed was the case of asperity contact with rigid or elastic asperities randomly distributed on a two-dimensional crack surface. Compact Tension geometry was assumed. For this work, micromechanical approaches were introduced as the basic means to obtain physically-based expressions calculating the forcing function at the crack tip. This method was employed because it provides a way of connecting to the results of the XTM experiments in measuring the effects of crack closure. In addition, stereological techniques were used to provide additional input required to characterize the three-dimensional nature of fracture surface and to represent the most salient measurable features on the actual fracture surface in two-dimensional form. Here, the most significant accomplishments were:

1. The characterization of the roughness-induced crack closure by the fractographic analysis.

2. Justification of the crack tip stress parameter, K, as a forcing function at the crack tip in the roughness-induced crack closure problem.

3. Development of analytical models to predict the closure stress intensity factors as a function of the crack length using a "phenomenological approach".

4. Investigation of the relations between fractographically measured parameters and the crack driving forces.

II. Fractographic Analysis

The motivation for this analysis is to answer the questions "What is the nature of roughness-induced crack closure?" and "What aspect of roughness height most significantly affects crack closure measurements?" or equivalently "What is the relationship between the roughness height and crack driving forces?".

A. Microscopic Observations

As seen in Figs. 1.1 and 1.2, roughness-induced crack closure is evidenced by fracture surface contact. Fig. 1.1b shows an enlarged area of the contact point indicated in Fig. 1.1a. It can be seen that very fine particles and oxides (from EDX analysis) are exiting from the inside of the specimen. This process stops when the crack length increases to some value where there is a large degree of separation between the crack surfaces. In Fig. 1.2, an abraded area near the specimen surface is also

shown. This was observed on the outside of specimen during the test.

In addition to the contact observations made externally, several different contact patterns which occurred inside of the specimen, are shown in Figs. 1.(3-5). In Fig. 1.3a it can be seen that opposite faces are wedged open by the roughness formed due to cracking on crystallographic slip planes. In Fig. 1.3b it is clear that the fracture surfaces can be shattered and distorted due to contact each other. Figures 1.4a and 1.4b show that either large or small particles torn from the basic fracture surface can block the contact of the fracture surfaces. Figures 1.5a and 1.5b show that separated grain boundaries can also abrade each other in the direction of loading. The nature and location of these various contact mechanisms along the fracture surface are summarized in Fig. 1.6. The "wedged open" contacts are normally found near the notch tip area since well-defined crystallographic deformation occurs mostly at the early stage of crack growth. Grain boundary separation occurs when large values of K_{max} are reached. Therefore, this contact mode tends to appear near the crack tip area for large crack lengths. The various documented contact patterns can be viewed in terms of idealizing the contact problem (i.e. appropriately and realistically idealizing the actual roughness on the fracture surface) to facilitate computation of the forcing function at the crack tip. When this is done, the most effective closure mechanisms arise from either the "wedged opened" or "debris

blocking" contact patterns. These can be modified to idealized shapes in contact on the fracture surface and used to develop expressions for the forcing function.

B. Quantitative Fractographic Analysis

From the preceeding section, it is observed that the nature of the roughness on the fracture surface plays a key role on the contact of asperities. However, the mechanism of the asperity contact is not defined through knowledge of only the roughness on the fracture surface. A quantitative fractographic analysis was performed to more fully understand the nature and significance of asperity contact. The initial step is to obtain the crack profile on the sections perpendicular to the crack propagation direction. The procedure involves several steps such as cutting the fracture surface from the specimen, mounting it in epoxy, vertical sectioning, polishing, and digitization of the profile. These various steps are shown in Figs. 1.7 and 1.8. A very important step is to define the reference line on the crack profile using least square methods, since this serves as a base line or plane necessary to represent the roughness on the plannar crack surface. Using the reference line the roughnesses on various sections in the thickness or crack propagation direction can be compared each other, as shown in Figs. 1.9 and 1.10. Also this idealizes the three-dimensional features on the complicated fracture surface to a two-dimensional representation in which the

roughness has an average height on the plannar crack surface. The crack surface normally appeared to have mixed mode features. This concept, which is summarized in Fig. 1.11, clearly characterize the mixed mode fracture, i.e., modes I and II and mode I and III. In this representation, asperity contact can be considered to involve two components: (1) mechanical contact of asperities due to the roughness on the fracture surface and (2) mixed mode crack sliding displacements of the crack tip when the load is applied. Fig. 1.12 shows the deviation of the plannar crack (which involves Modes I and II) from the line perpendicular to the loading direction for one of the Al-Li 2090 specimens. The cracks for most specimens stayed in side groove and deviated within 5°, which is allowed in ASTM E-647 specifications. Mixing of modes I and III is shown in Fig. 1.13 by angular deviation. As the load range , ΔP, increases, the angular deviations, ϕ, also increase. However, the deviations oscillate about the same mean value as the crack length increases. From Figs. 1.12 and 1.13, it can be seen that the contributions of mixed mode fracture resulting from the sliding displacements vary with increasing crack length. The average roughness height increases regularly in the early stages of crack growth, but varies after reaching the mid-range of ΔK as shown in Fig. 1.14. This figure shows a possible relationship between the average roughness height and the nominal range of stress intensity factors for the different ranges of applied load and R-ratio used in this study.

III. K as a Forcing Function In the Crack Closure Problem.

The fundamental question is whether the crack tip parameter, K, can be used as a forcing function at the crack tip in the crack closure problem. Fig. 2 shows the finite element results for the change of stress around the crack tip with and without closure. From this, it is clear that the change of stress near the crack tip for both the non-closure (slope A) and closure (slope B) varies linearly with the inversely square root of distance from the crack tip. Also, slope B is smaller than slope A, which indicates the forcing function is reduced due to the crack closure. Therefore, the stress intensity parameter, K, appears to be a valid parameter to represent the change of stress distribution when crack closure occurs.

IV. Analytical Modeling of Closure Stress Intensity Factors as a Function of Crack Length.

The goal of this work is to predict the variation of closure stress intensity factor as the crack length or the maximum of the range of stress intensity factor increases for constant applied load. A recent study by J.E. Allison, (1988) provides some schematic variations of closure for different closure mechanisms as shown in Fig. 3.1. As seen from the figure, two different curves are hypothesized for asperity contact: one is constant (for most titanium alloys) and the other is decreasing reversed-exponentially (for some ferrous alloys).

The following "phenomenological approach" is suggested in order to predict analytically the variation of closure stress intensity factors. This method uses the closure load, P_{cl}, as determined by extrapolating two compliance curves and finding the intersection as shown in Fig. 3.2a. Then a parameter, V_{cl}, corresponding to the closure load is introduced as a "representative" closure crack opening displacement. From the fractographic analysis, it was observed that the most asperity contact occurs in the wake zone behind the crack tip. Then the closure stress distribution in this area may be in the form of tailing off equation, which is shown in Fig. 3.2b. If the distributed contacts are converted to a single contact by an imaginary equivalent asperity,the "representative" closure crack opening displacement corresponds physically to the crack opening displacement which occurs at the location of the single asperity,C_{cl}.

Two different models are suggested to predict the variation of the closure load with crack growth, as shown in Fig. 3.3. In model A, when the crack grows, the new contact distance,C'_{cl}, would be assumed to be the distance linearly increased by an amount equivalent to the increase in crack length. In model B, the new contact distance is assumed to be independent of the increment in crack growth. Assuming that the mechanism of crack closure opening displacement at asperity contact remains unchanged, the new closure load must be reduced in order for the new contact to occur at C'_{cl}. This conceptual model predicts a

variation of the closure stress intensity factors as shown in Fig. 3.4. The only difference from the hypothesis made in the previous study is that model A predicts an exponentially decreasing value with crack extension. As shown in Figs. 3.5 and 3.6, the predictions of model A appear to be well correlated to experimental data obtained for Al-Li Alloy 2090. Here, the analytical result was obtained for $C_{cl}=C_1 a$, where a is a crack extension, and C_1 is experimentally observed to be less than 0.3.

V. Conclusions

The most significant contributions of this work lie in developing a more in-depth understanding of asperity contact mechanisms by means of direct observation and quantitative fractographic analysis and incorparation of this information into the development of quantitative models for crack closure. Also the finite element analysis clearly shows that the crack tip stress parameter, K, can be used as a valid parameter to represent the stress change around the crack tip due to the asperity contact. With some experimentally observed information, the analytical model predicts closure stress intensity factors which correlate well with experimental data.

a)

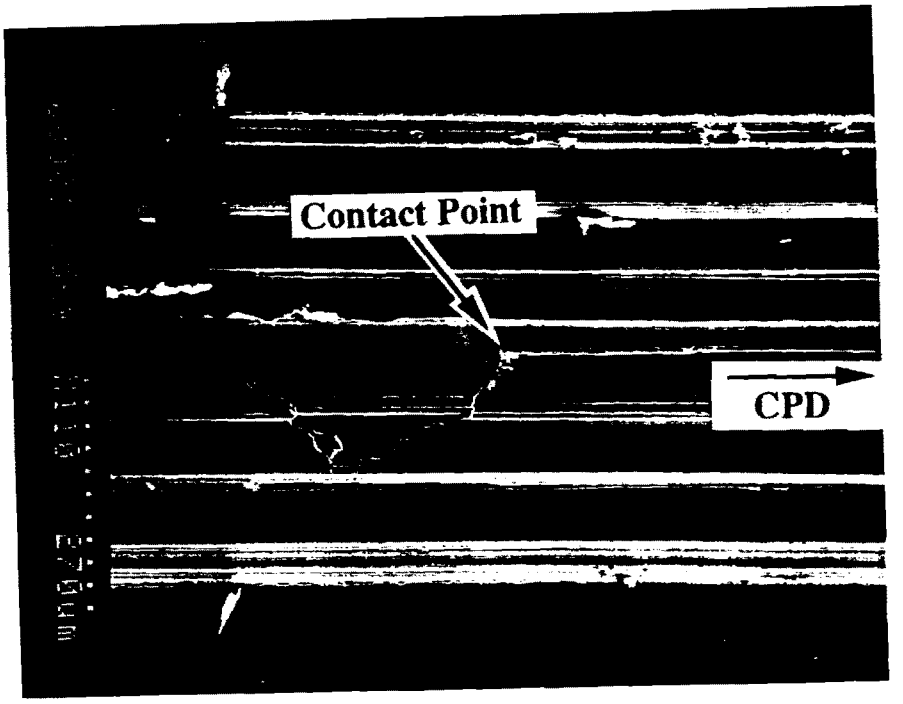

b)

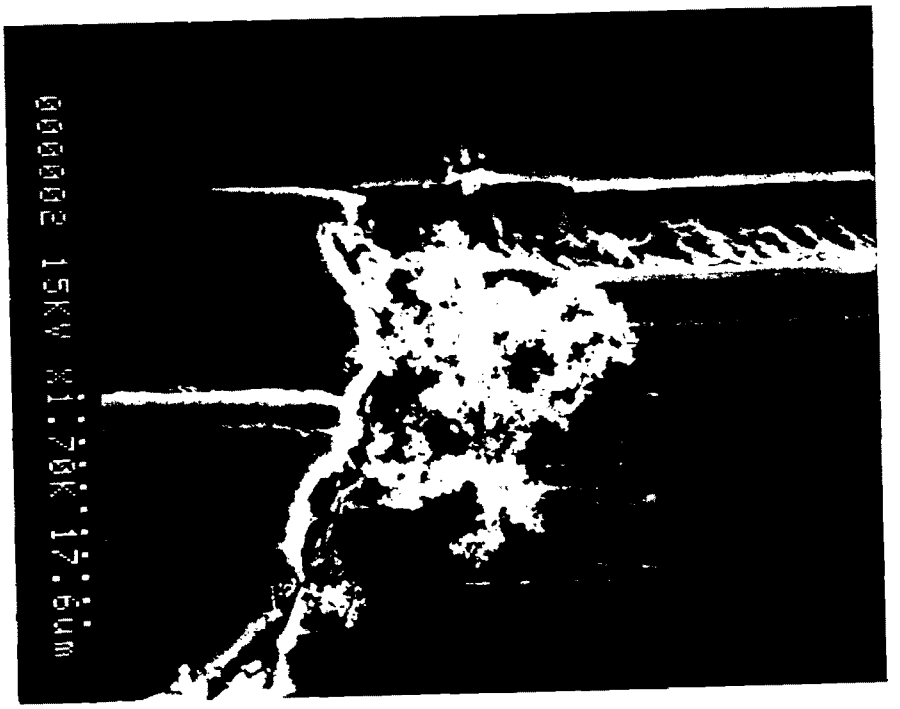

Figure 1.1: a) Fracture surface contact at the kinked point. "CPD" means the crack propagation direction.
b) Enlarged area of a).

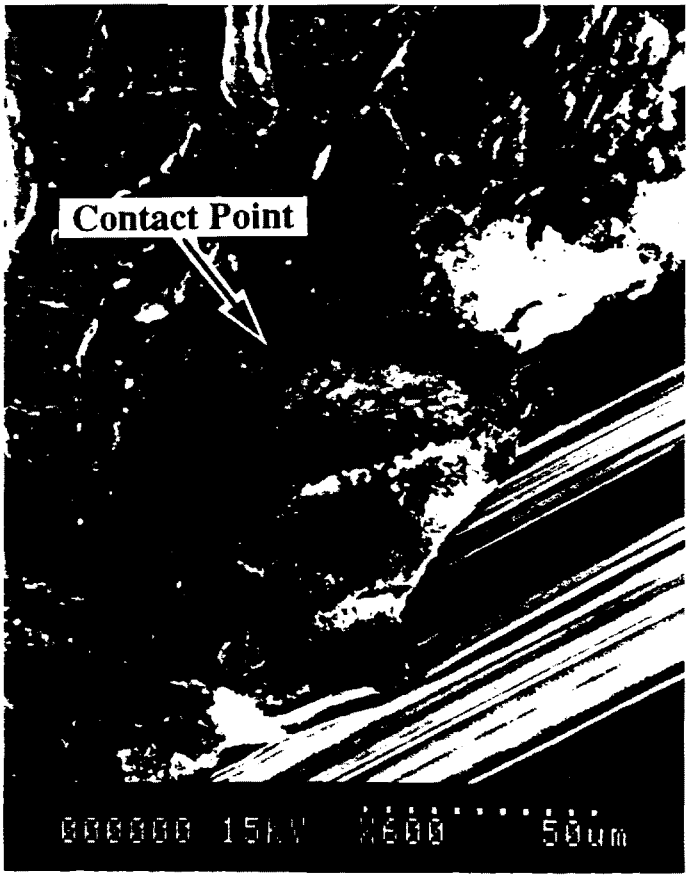

Figure 1.2: Abraded fracture surface on the inside of the specimen at the contact point of a).

a)

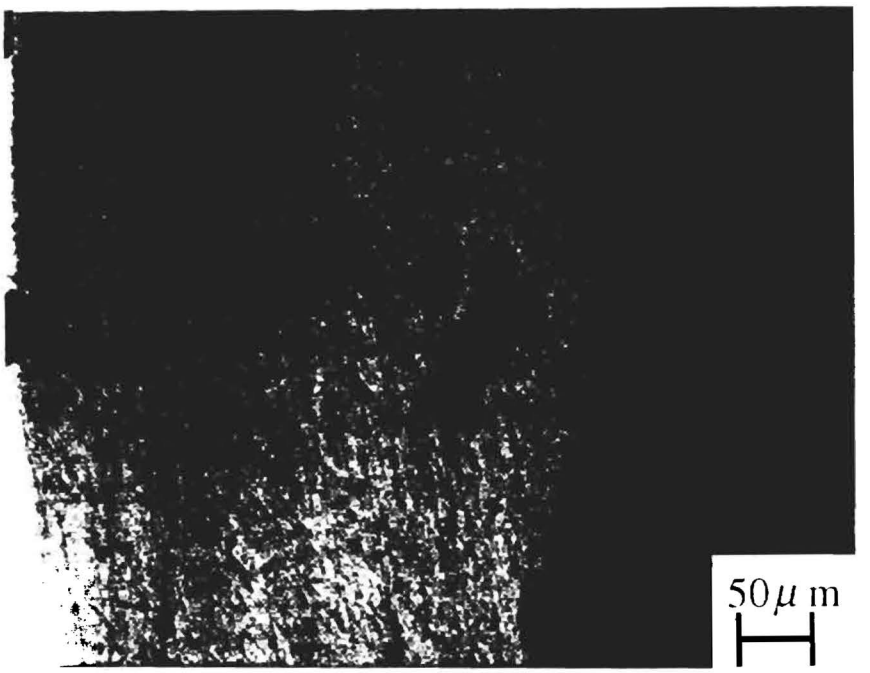

b)

Figure 1.3: a) Opposite faces are "wedged open".
b) Fracture surfaces are shattered and distorted due to contact each other.

a)

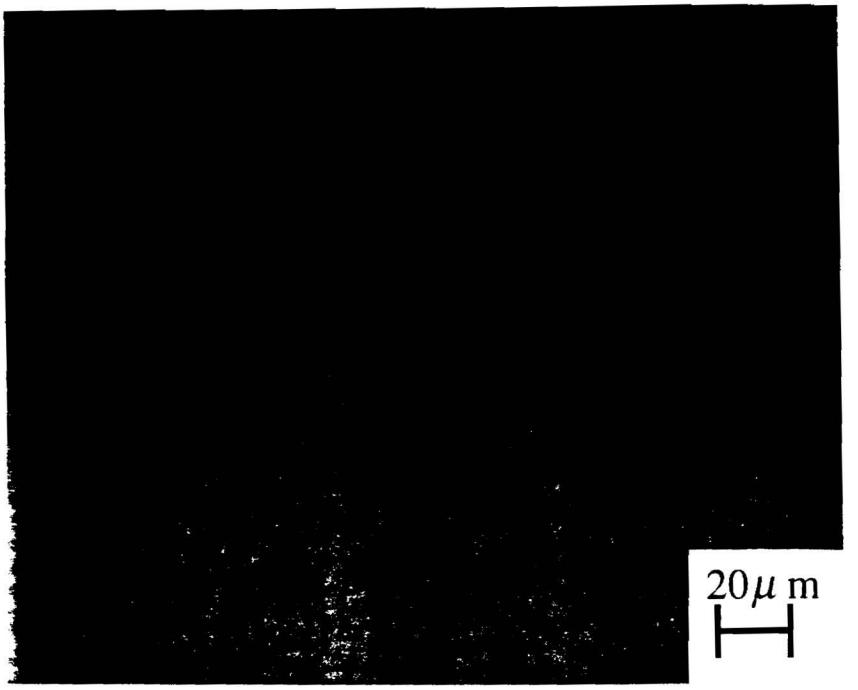

b)

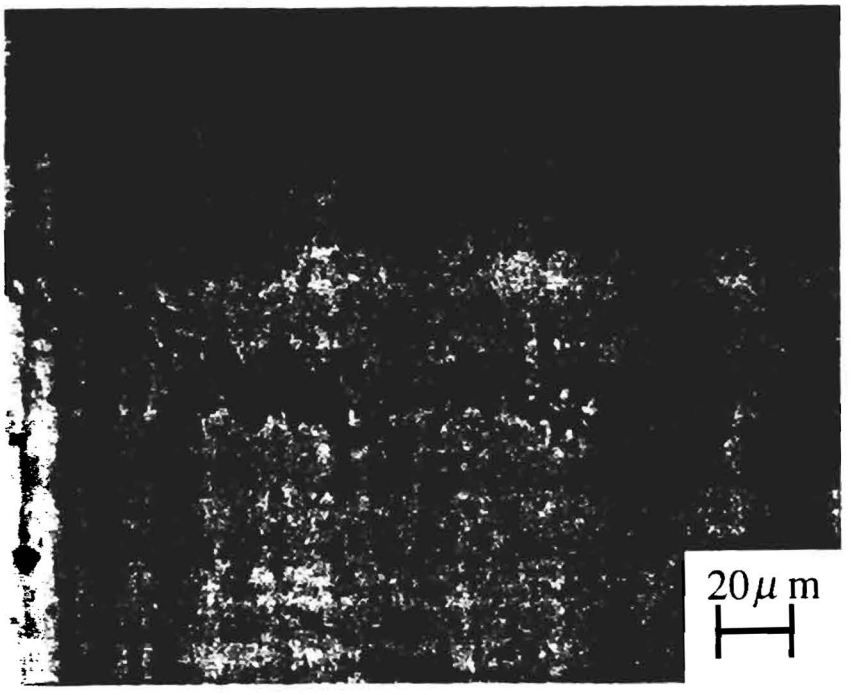

Figure 1.4: Either a) large or b) small particle torn from the fracture surface blocks to contact of surfaces.

a)

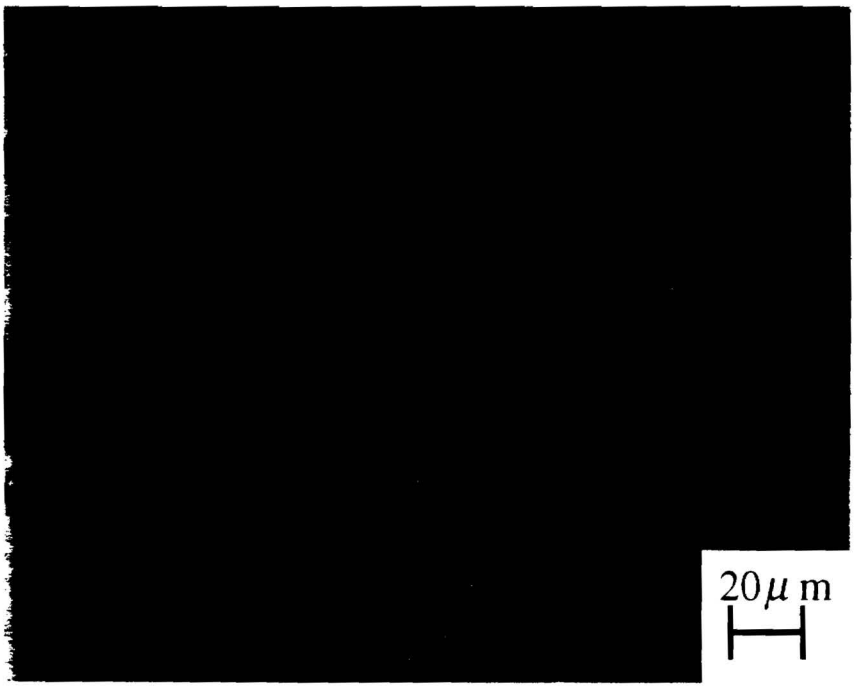

b)

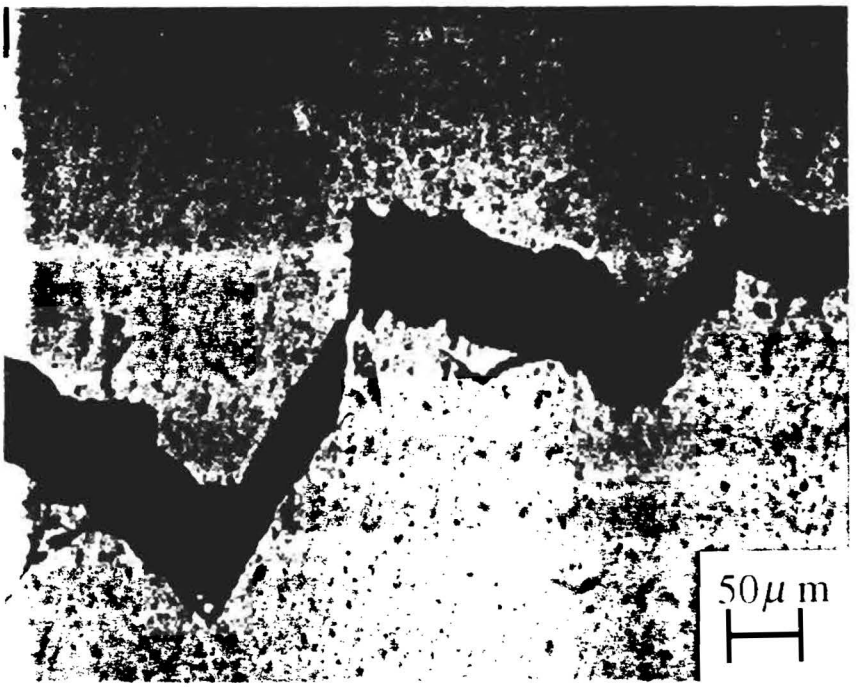

Figure 1.5: Separated grain boundaries a) abrade or b) contact in the direction of loading.

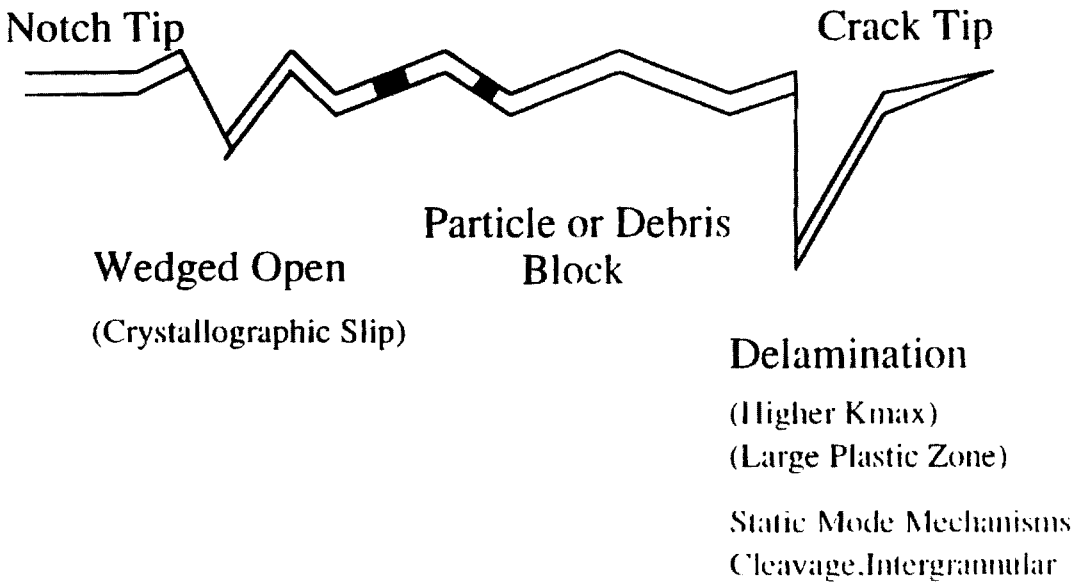

Figure 1.6: Schematic view of various contact mechanisms along the fracture surface.

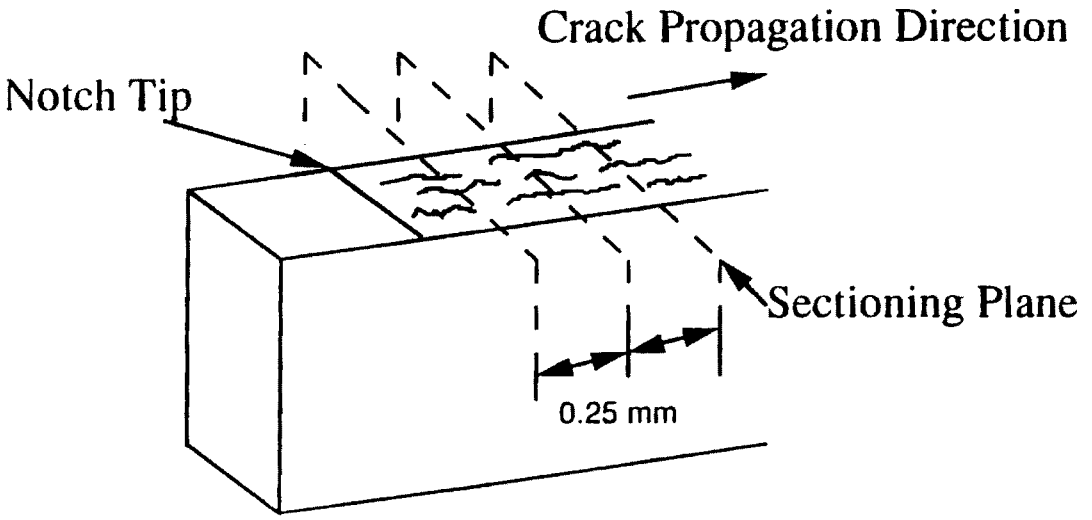

Figure 1.7: Sectioning scheme of fracture surface in the direction of crack propagation.

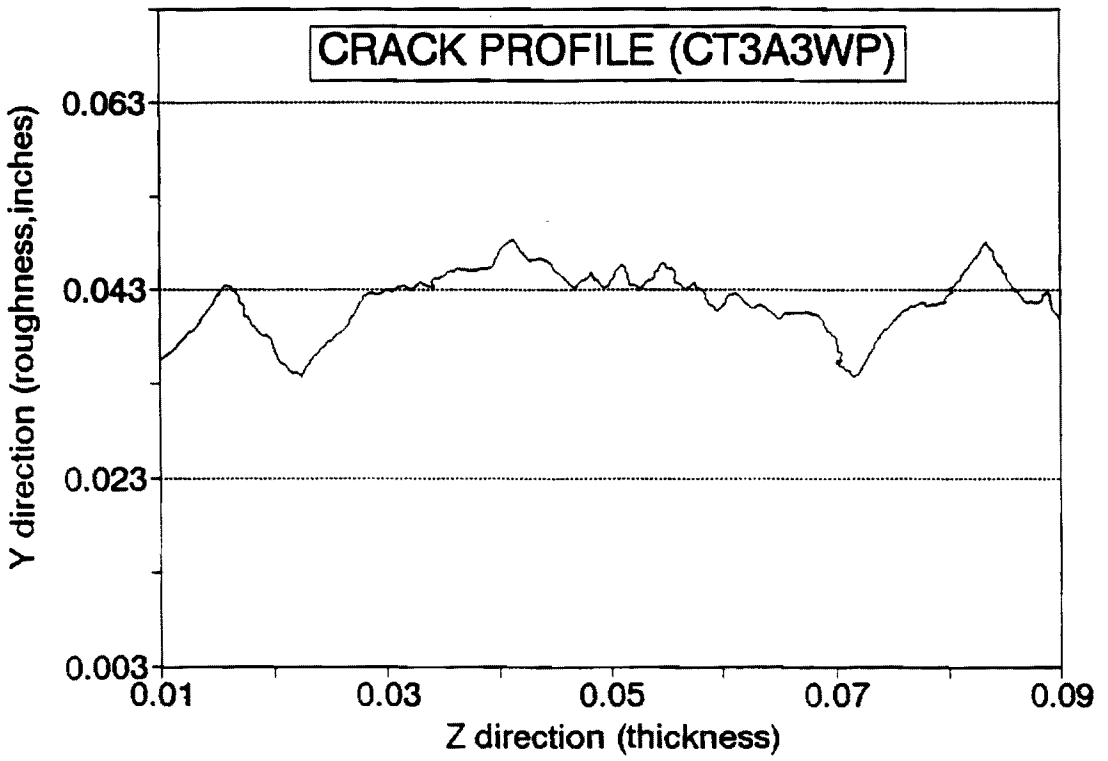

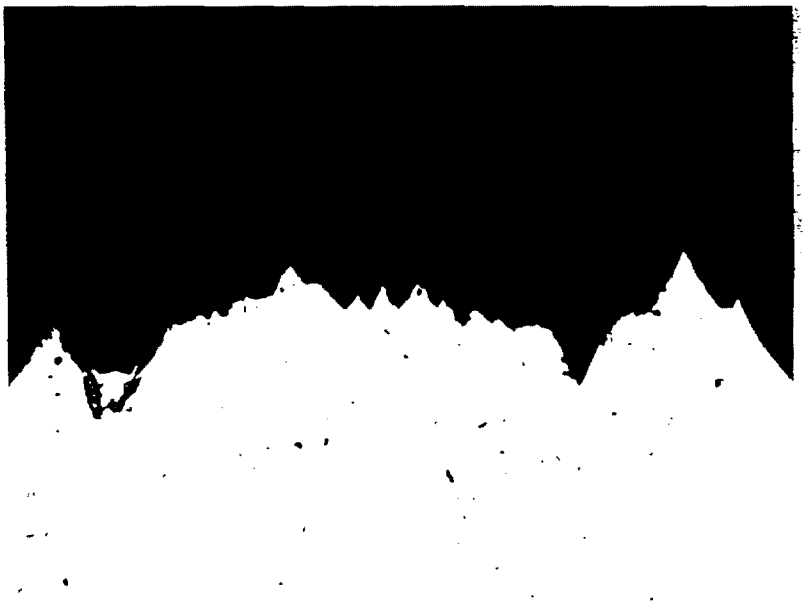

Figure 1.8: Digitization of crack profile of which dimensions are actual.

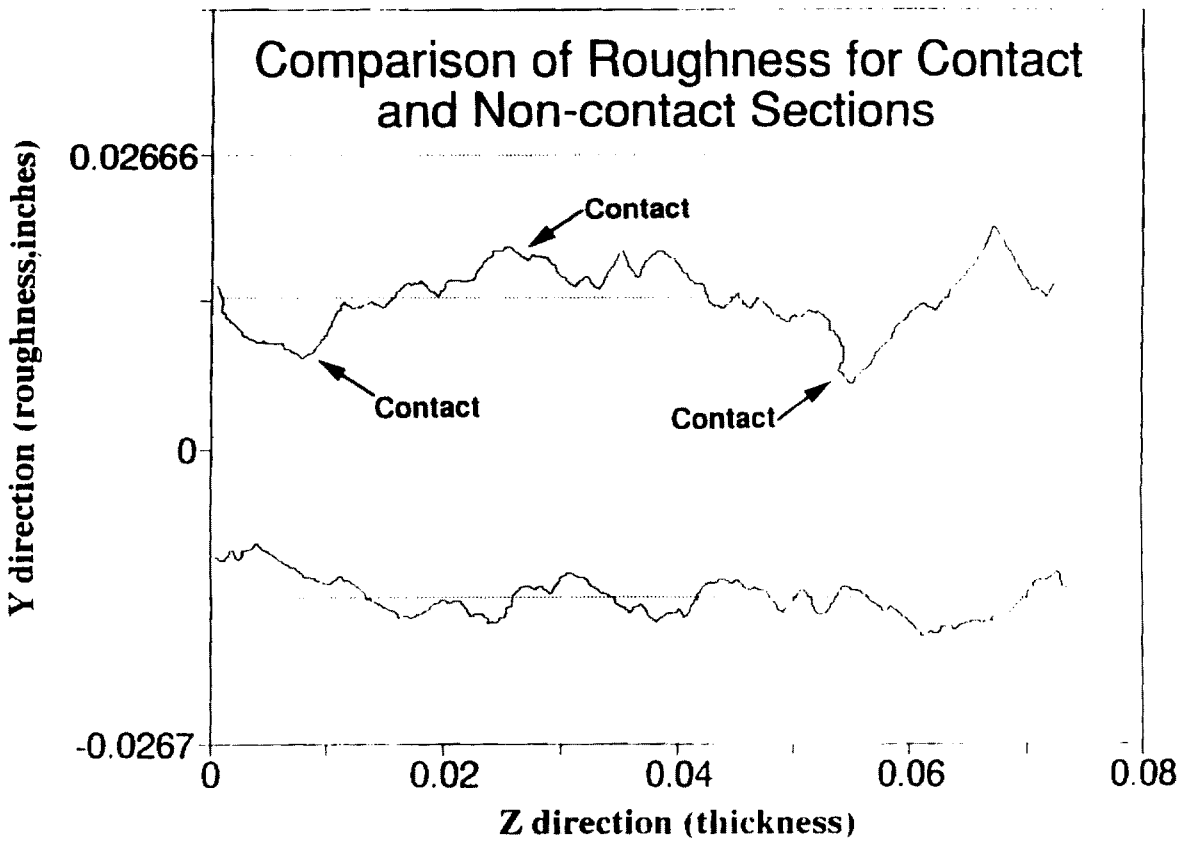

Figure 1.9: Comparison of roughness on contact and non-contact sections in the thickness direction.

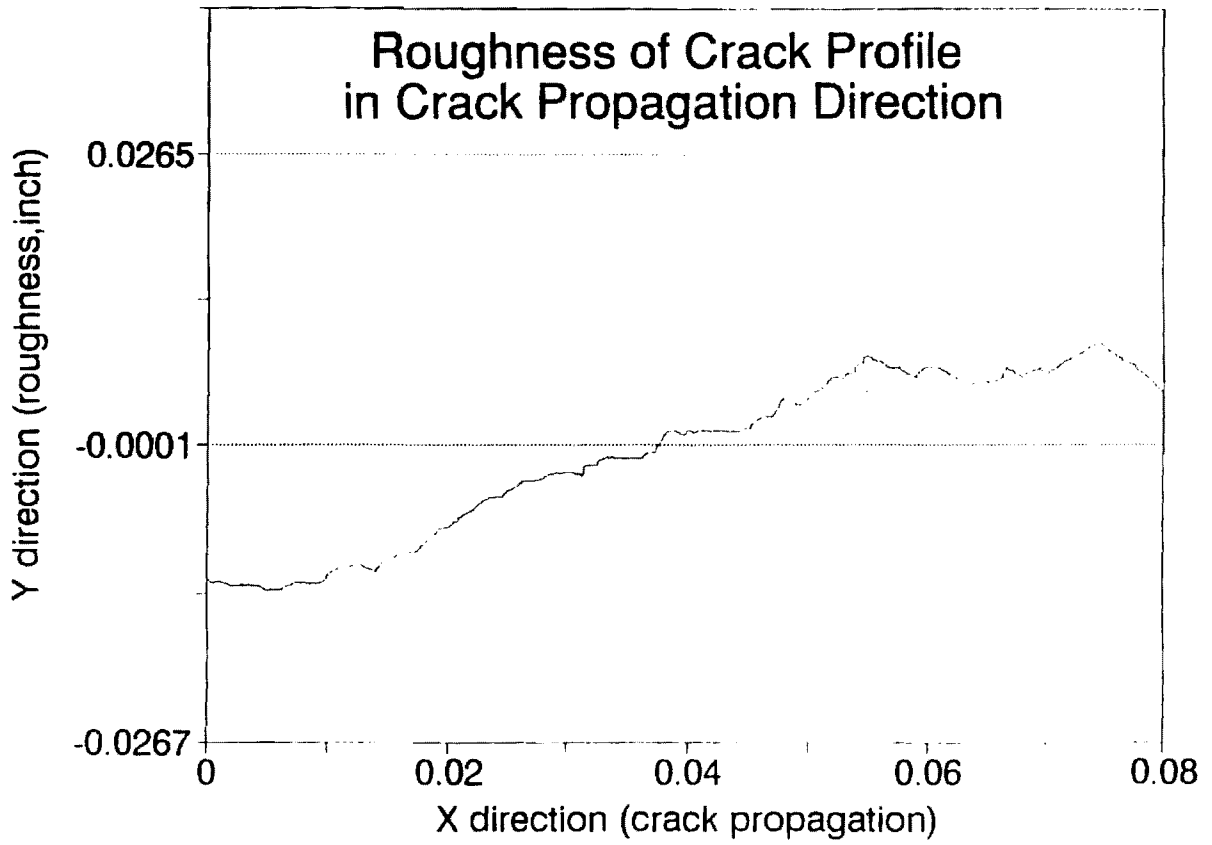

Figure 1.10: Roughness on the fracture surface in the crack propagation direction.

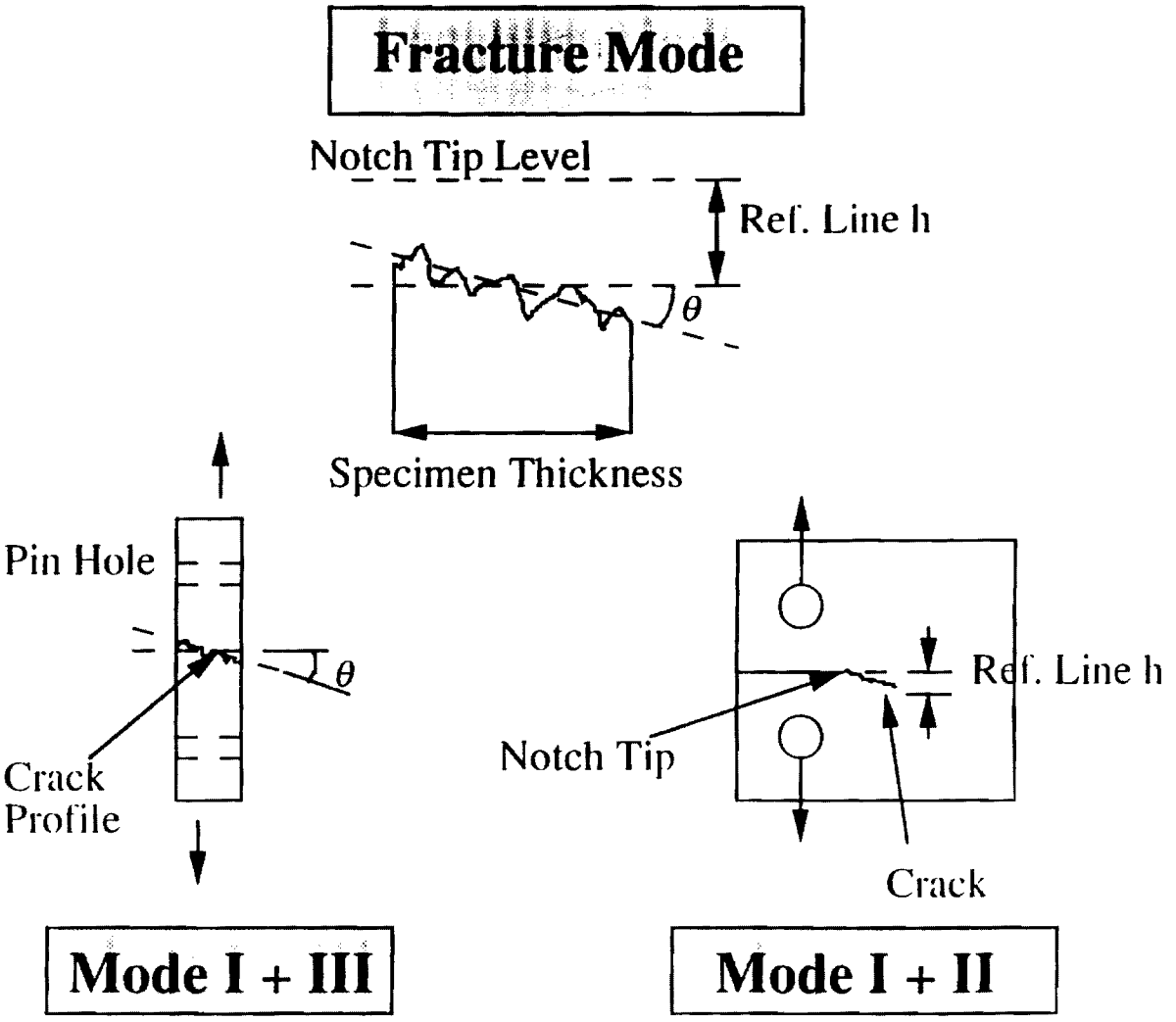

Figure 1.11: Characterization of the mixed mode fracture by fractographic analysis.

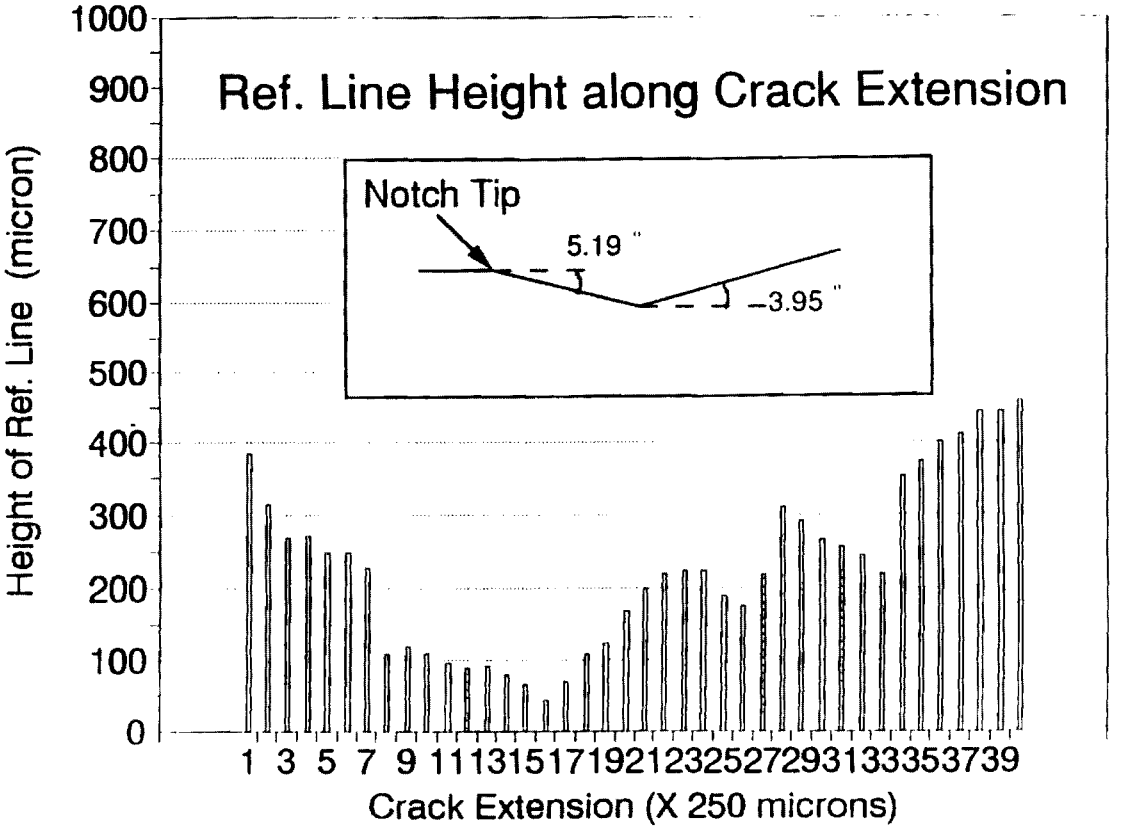

Figure 1.12: Deviation of the planar crack (Mode I and II) along the crack extension.

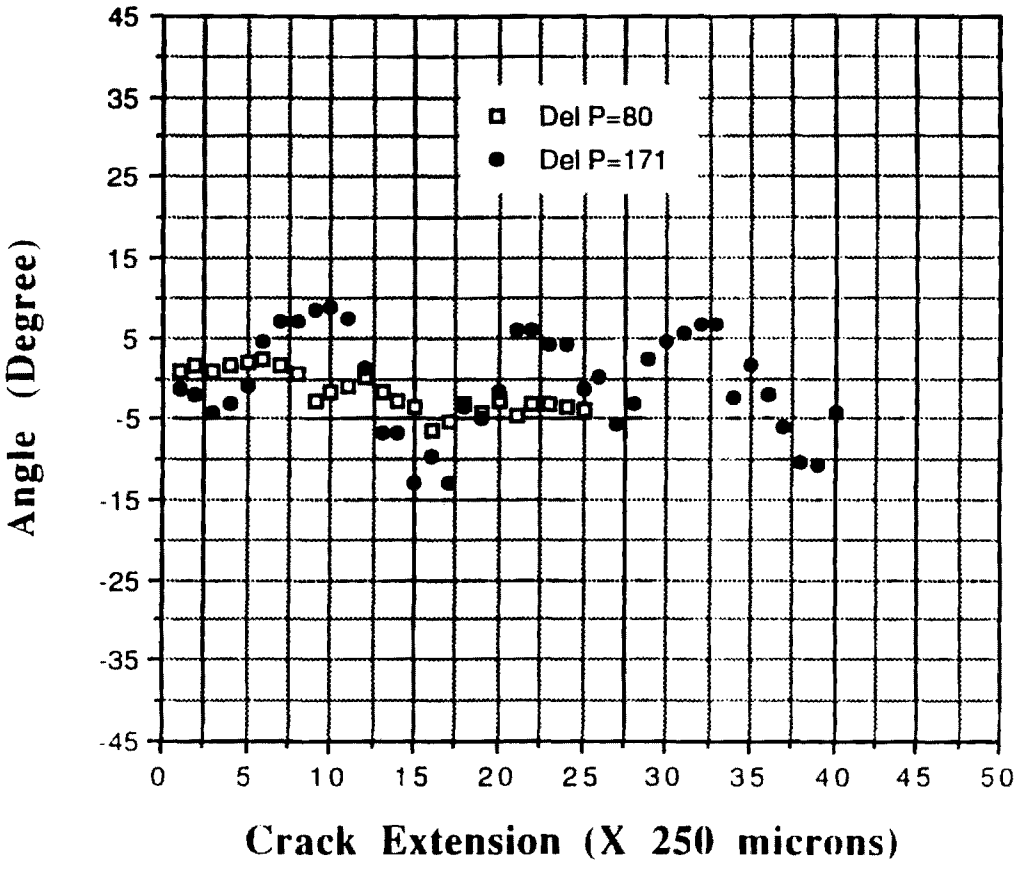

Figure 1.13: Representation of mixing of Mode I and III by angular deviation along the crack extension.

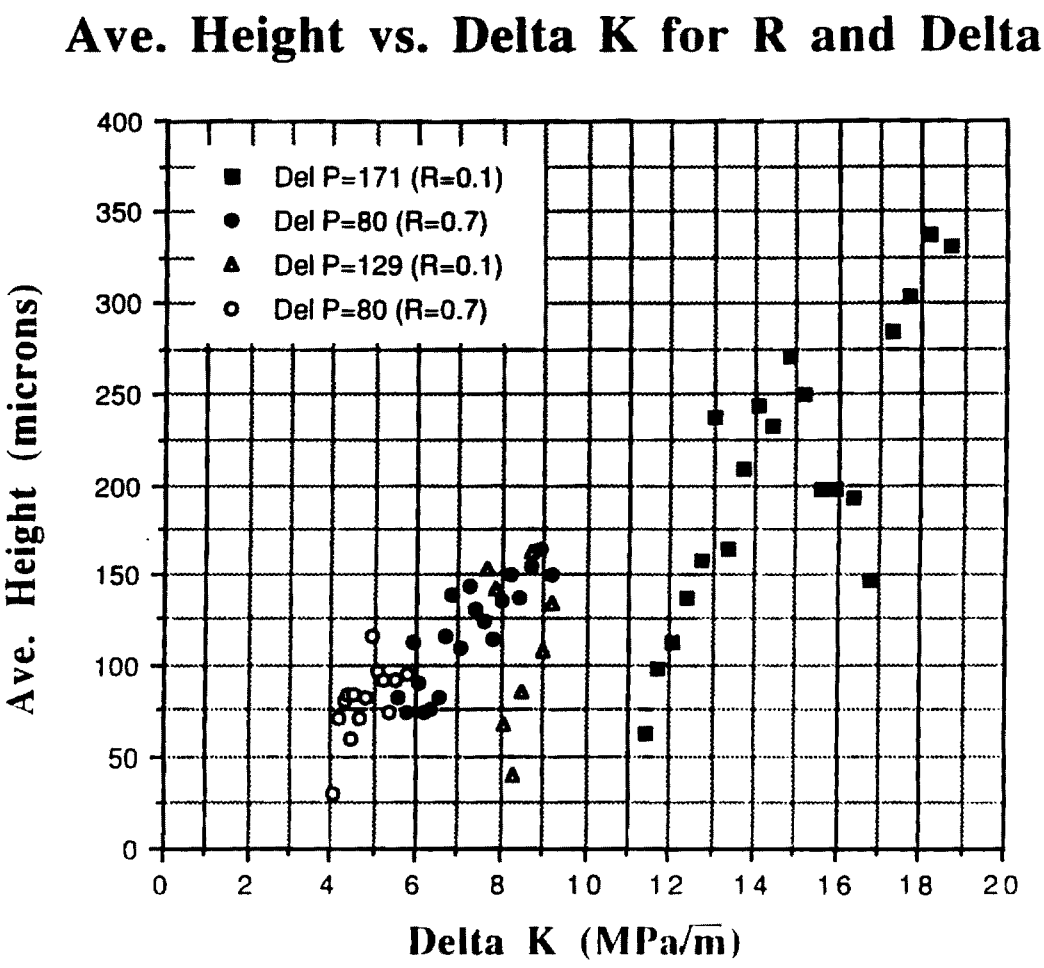

Figure 1.14: Average height of roughness versus the nominal range of stress intensity factors.

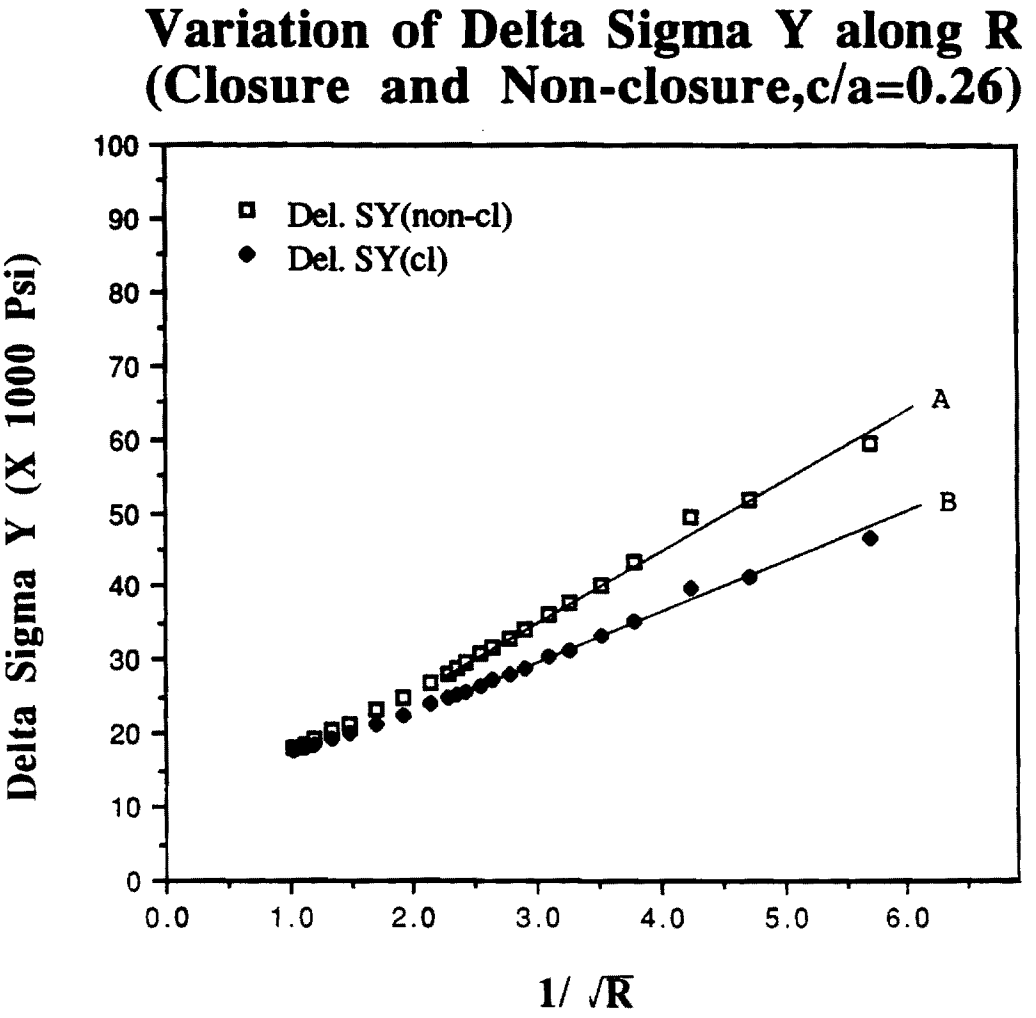

Figure 2: The change of stress near the crack tip with and without closure versus the inversely square root of distance from the crack tip.

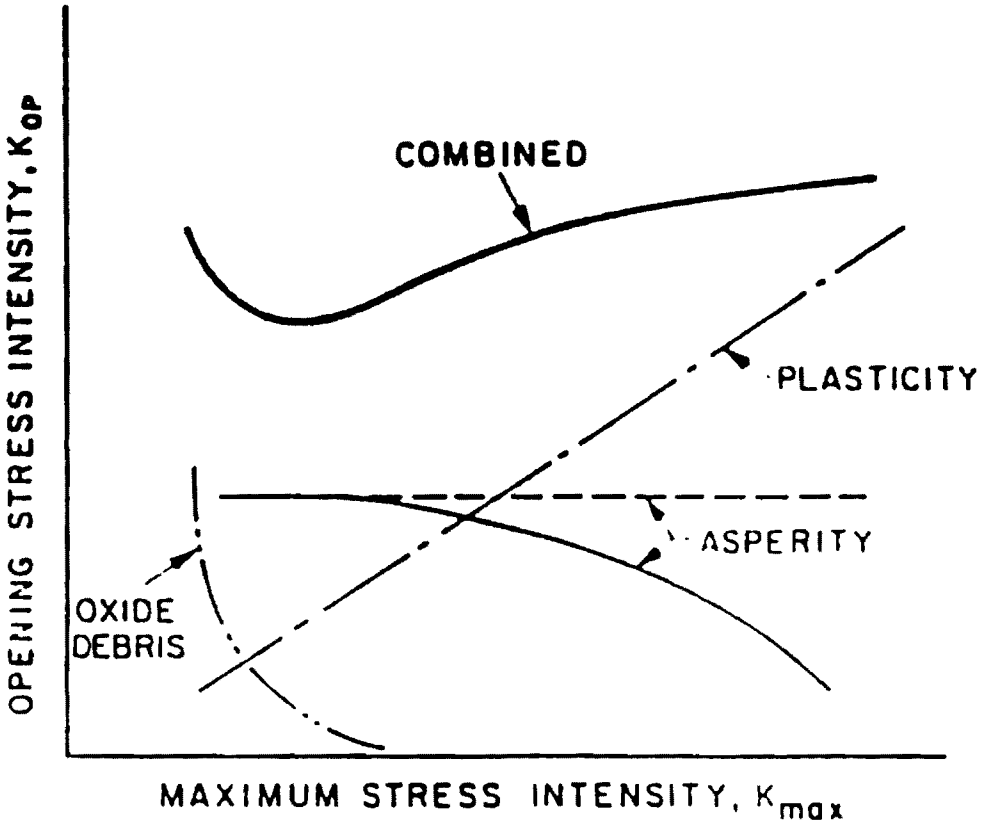

Figure 3.1: Schematic variations of closure for different closure mechanisms. (J.E. Allison, 1988)

a)

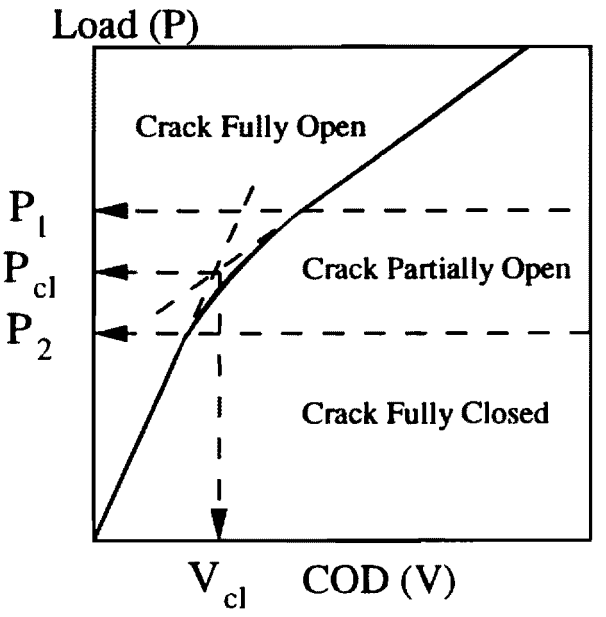

b)

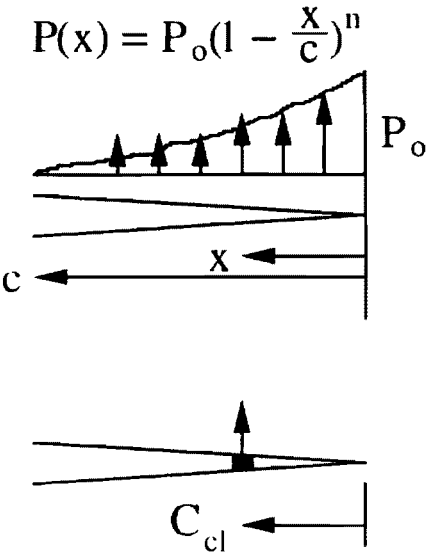

Figure 3.2: a) Determination of closure load, P_{cl}, and "representative" closure crack opening displacement, V_{cl}, by extrapolating two compliance curves.
b) Closure stress distribution in the wake zone behind crack tip.

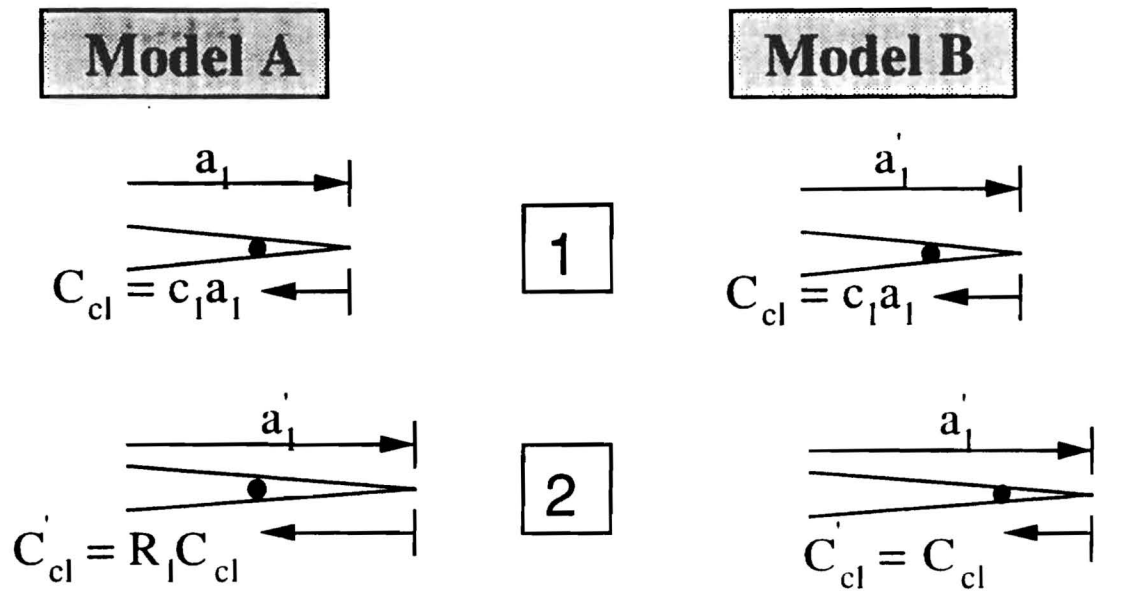

$$R_1 = \frac{a_1'}{a_1} = \frac{a_1 + \Delta a}{a_1}$$

$$R = \frac{V_{cl}^2}{V_{cl}^1} \qquad P_{cl}^2 = \frac{V_{cl}(a)}{R} P_{cl}^1$$

Figure 3.3: Schematic view of models predicting the variations of the closure load with crack growth.

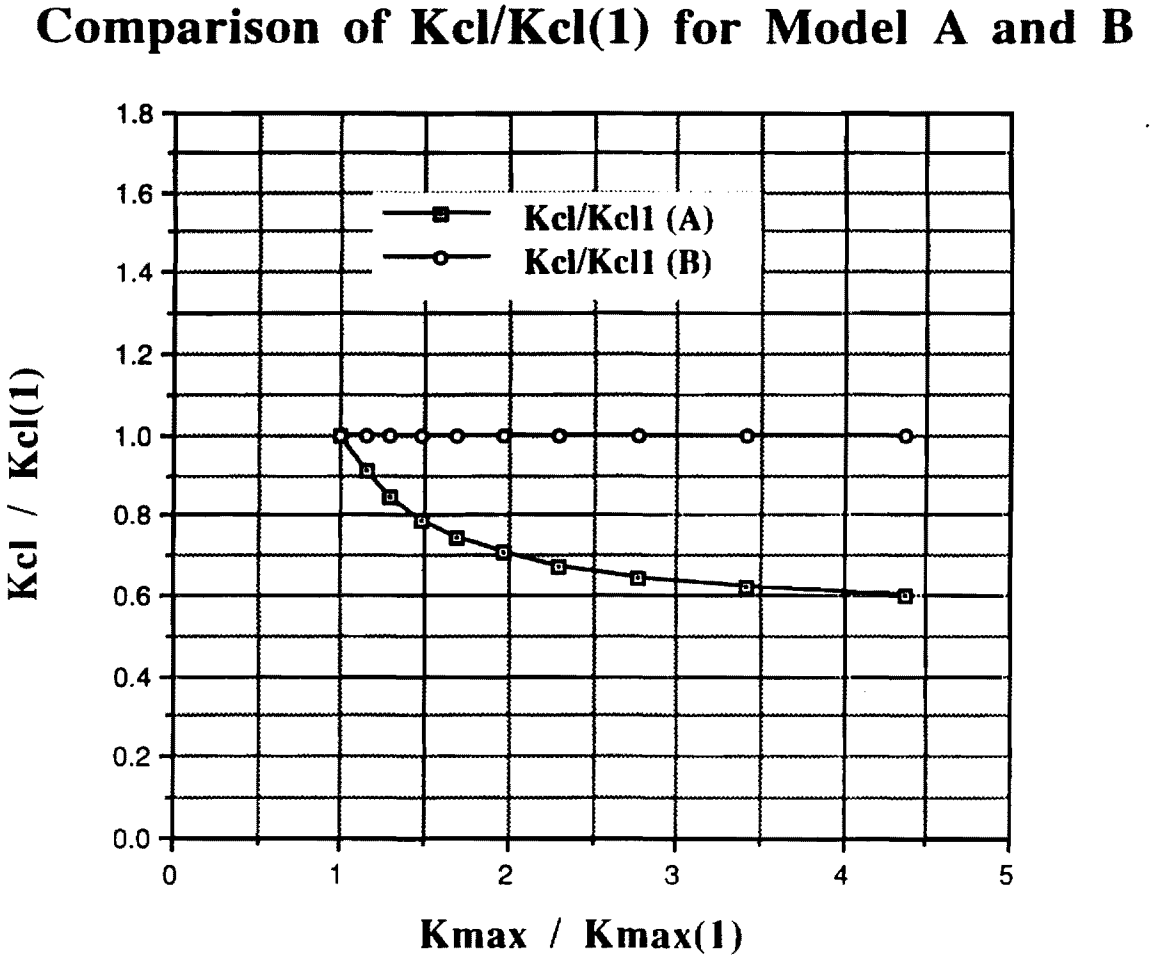

Figure 3.4: Variation of normalized closure stress intensity factors along the crack growth. $K_{cl}(1)$ and $K_{max}(1)$ are the first measured K_{cl} and K_{max}, respectively.

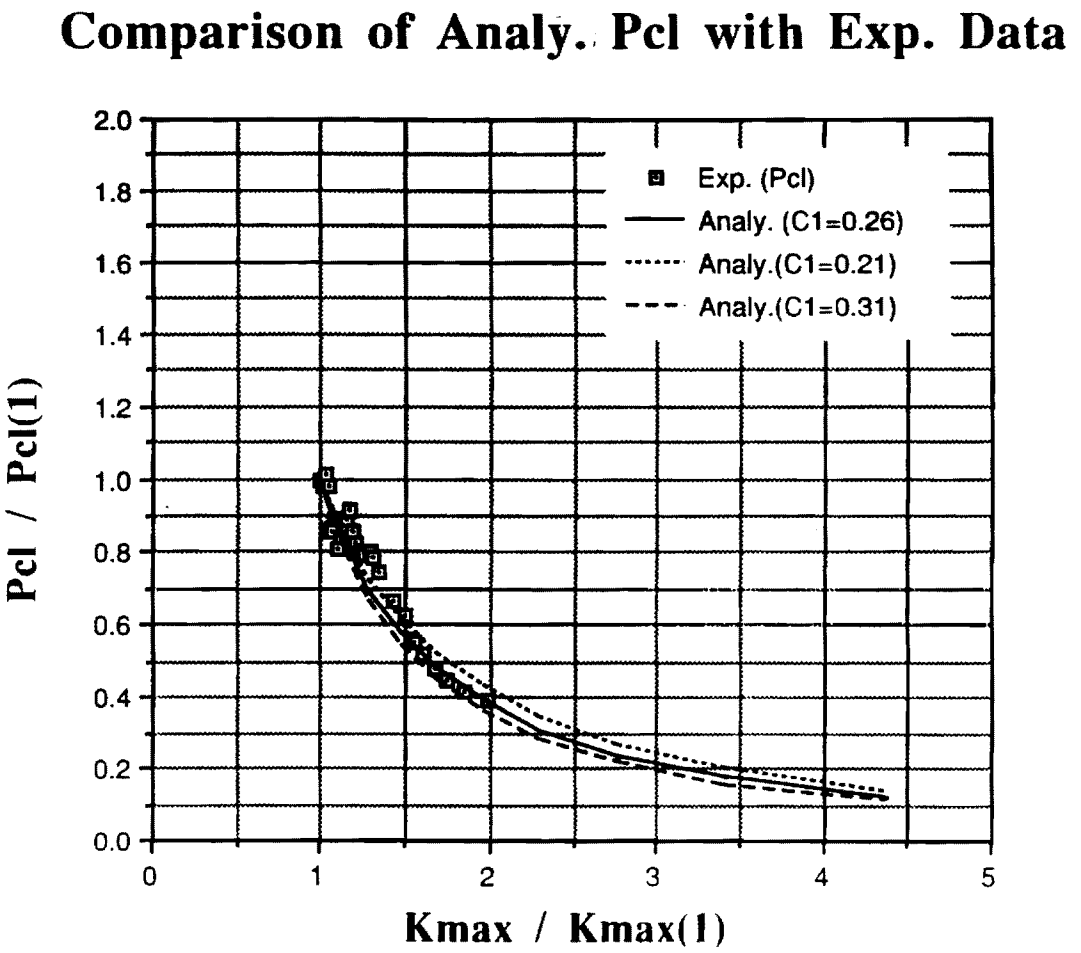

Figure 3.5: Comparison of analytical closure load in model A with experimental data.

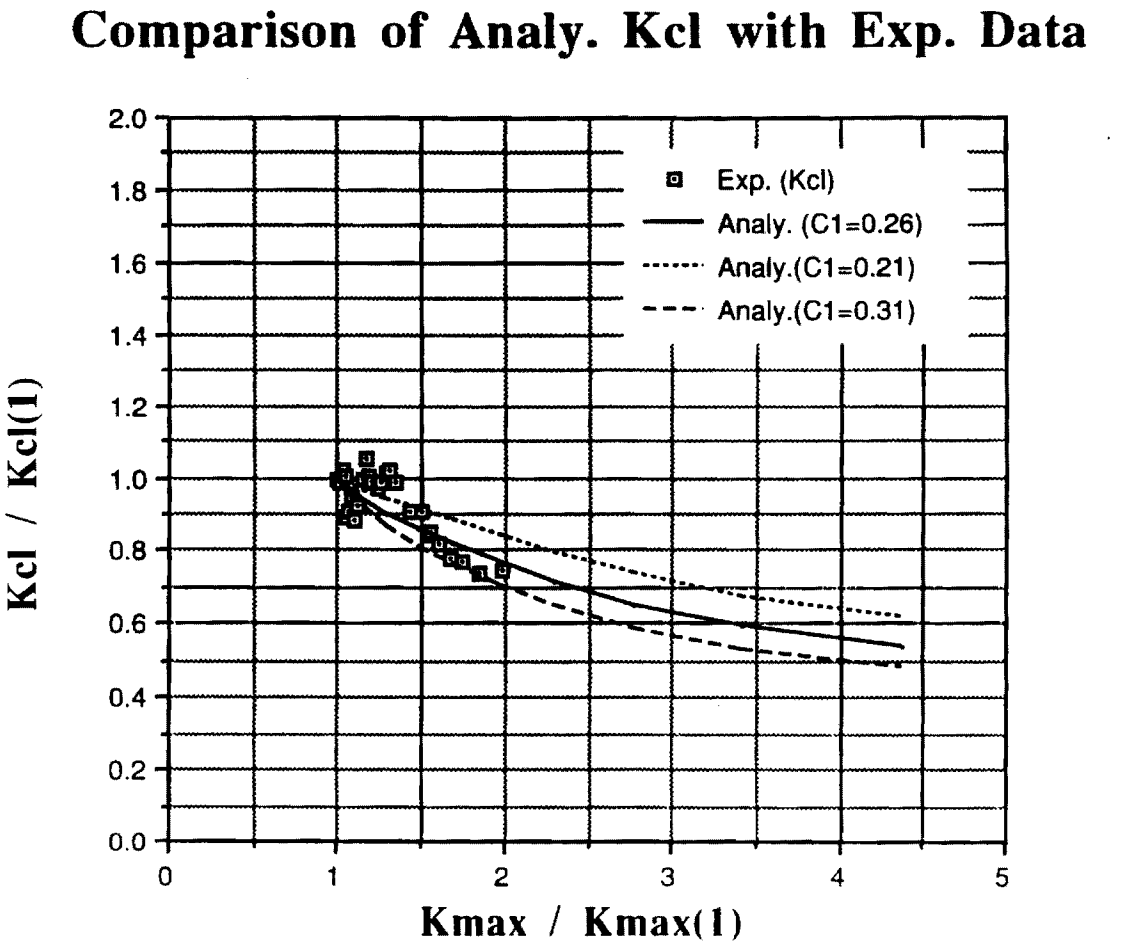

Figure 3.6: Comparison of analytical closure stress intensity factors for various C_1 values with experimental data.

Part B. I. Introduction

The goal of observing crack face interactions in the interior of intact samples was accomplished using very high resolution x-ray computed tomography. Two notched tensile and one compact tension samples were imaged under load using a miniature load frame designed for use with computed tomography under this program. New methods were developed for measuring the amount of opening as a function of position for different applied loads. Two schemes for presenting the crack opening data as a function of position were devised in order to allow one to emphasize the position of the crack tip or to clearly observe the geometry of the surfaces coming into contact at different loads.

II. Direct Observation of Physical Crack Closure

The experiments in which the notched tensile samples (NT-3 and NT-4) were imaged have been discussed in earlier reports, and, for brevity, this will not be repeated here. Two additional imaging experiments were performed on a compact tension sample (CT-2). The first set of measurements were made with the Air Force Materials Laboratory's Tomography system (in collaboration with Air Force and ARACOR personnel, the Air Force's on site contractors). The second was with the high resolution digital radiography apparatus at Lockheed Missiles in Palo Alto, CA. Both were successful in showing changes in crack opening as a function of position and applied load. Only the results from Lockheed are discussed below: the volume element (voxel) size with the ARACOR system was

considerably larger than the isotropic 20 μm pixels obtained in the reconstructed Lockheed data.

Fatigue crack growth rates in sample CT-2 and the other samples tested were essentially identical with those reported in the literature for full-sized compact tension samples. After pre-cracking of CT-2, its crack length was 5.6 mm, and at the end of the test, after 651,080 cycles, the crack tip was about 15.2 mm from the load line (i.e., with W = 25.4 mm, the remaining uncracked ligament was about 10.2 mm). The corresponding stress intensity ranges were 15 and 19 MPa$\sqrt{m}$, respectively. The reader should note that P_{max} was initially 106 kg and it was decreased periodically to prevent unstable crack growth.

The Lockheed x-ray system was used in the following configuration: a 2048 x 2048 x 12 bit fiber-coupled camera system was used with a 10 μm focal spot of a Kevex microfocus source operated at 160 kV and 0.06 mA and with a geometrical magnification of 1.8. Images were acquired at 359 angles (the rotation axis was parallel to the stress axis), each radiograph was recorded with 10 sec exposure and the volume containing the crack was reconstructed with isotropic 20 μm voxels using the Feldkamp cone beam reconstruction algorithm. Data was collected at five applied loads: 42, 35, 28, 21 and 8 kg (approximately 92, 77, 62, 46 and 18 lbs). The maximum load was that the sample experienced during the final increment of crack growth.

The load-displacement curve for sample CT-2 was recorded using a laser extensometer after the x-ray imaging. The curve is shown

in Figure 1 with the loads at which tomography was performed labeled by arrows and the letters a-e. The closure load, determined by linear extrapolation of the upper and lower ranges of the curve, is seen to be about 16 kg (35 lbs).

From the reconstructed data, the three-dimensional volume of material containing the crack can be numerically sectioned along any arbitrary plane. In the case of sample CT-2, visualization is best (and comparison of the crack within the same volume of material at different loads is most precise) if one numerically sections along the planes containing the stress axis and the sample face (Figure 2): in other words, the cuts span the sample thickness from one face to the other, and the side-grooves appear in the left and right of each cut separated by 1.75 mm. Figure 2 shows every tenth cut, i.e., the 20 μm thick cuts of material are spaced by 200 μm, at the highest load. The numbers in the lower left of each cut give the cut's distance in mm from the notch tip. Darker pixels correspond to voxels with lower absorption, the tips of the two side-grooves (1.75 mm apart) are visible at the left and right center of each image and the stress axis is vertical.

The series of cuts reveals that volumes of asperity-dominated crack geometry alternate with relatively planar sections of the crack. Considerable crack branching is visible throughout. The multiple asperities in the material nearest the notch give way to a single large asperity (seen near the left side-groove in cuts 0.3 through 1.1) on one side of a relatively flat crack. The gentle waviness of the crack continues between 1.3 and 3.1 mm, with the

crack inclined at a slight angle to the surface in cuts between 1.3 to 1.9 mm, a transition region where the crack bows concave up and the crack running directly across the sample between cuts 2.3 and 3.1 mm from the notch.

Multiple asperities dominate the crack geometry from 3.3 to 6.1 mm. After this the crack becomes relatively flat until 8.1 mm where the asperities appear to become important once again. The contrast from the crack begins to disappear beyond 8.3 mm for cuts at 8 kg load, but at 42 kg load the crack is visible across the entire cross section until about 8.6 mm. Some discontinuous-appearing sections of the crack are seen until about 9.6 mm, which is about the maximum extent of the crack seen in carefully aligned radiographs, but the contrast of the crack differs little from the noise in the image surrounding it. The compliance measurements indicate that the crack extended about 9.7 mm from the notch, which is in good agreement with the tomographic results. The sample is still intact, so that no further comparisons can be made between the actual crack surface and the tomography results.

Crack opening as a function of position was measured numerically for the maximum and minimum loads, and the procedure consists of several steps. First the average value of the linear attenuation coefficient μ_{avg} of the voxels of uncracked material was determined away from the crack, and any voxels with $\mu < 0.9\mu_{avg}$ were identified as potentially being partially or totally occupied by a crack. The approximate position of the crack was marked manually, and the value of each voxel above and below the approximate center

of the crack was checked until a value of $\mu > 0.9\ \mu_{avg}$ was encountered. The partial volumes of crack in the voxels between the two limits were then summed to give the total crack opening.

Figure 3 shows two pairs of cuts at the maximum and minimum loads (42 and 8 kg, respectively), and this clearly shows the amount and location of the physical crack closure. The location of the top and bottom pairs of cuts are 2.96 mm and 5.12 mm, respectively, from the end of the notch, and these are used to illustrate measurements for different crack morphologies. The total crack opening at each position is shown in the plot below each pair of cuts; the uppermost curve gives the opening at the higher load. Across the two thin volumes of material, there is considerable variation in crack opening and in the amount the opening changes (which gives the amount by which the two crack faces have moved together). In these two cuts the flatter areas of the crack tend to be more open, and subtle differences with position in a single cut are seen in the amount of crack closure. At other locations which are not shown here, however, large differences in crack closure are seen in adjacent areas of the crack. Openings from crack branches away from the main crack are not included here. When crack branching is seen, the crack openings of the branches are recorded separately for further analysis.

Two different methods have been employed to show how crack opening varies as a function of position over the entire crack. In the first, the measured crack opening is projected onto a plane.

This show quite directly how the crack tip closes as the applied load decreases. Figure 4 shows this type of representation for notched tensile sample NT-4: increasing amounts of opening are indicated by the progression of colors black, red, blue, green and white.

It is also possible to combine the three-dimensional topography of the crack with the opening measured at each position. In order to understand this scheme, one should first consider a three-dimensional representation of crack position within the interior of the sample (Figure 5 shows a three-dimensional mesh plot of the crack's surfaces). The notch is at the left, and the plot extends about one-half of the distance between the notch tip and backface. The crack extends somewhat farther than is shown in Figure 5, but quantification of opening beyond the positions shown cannot be done reliably over continuous stretches of the crack because of the small amount of opening produces changes of contrast comparable to the noise in the data.

One should note that the contour lines show the relative height of different portions of the crack surface in representations such as Figure 5. One can quite simply superimpose a color-table map of crack opening (such as in Figure 4 for a notched tensile sample) onto the three-dimensional image of the crack "plane." The result is Figure 6, where the colors represent the amount of opening at each position on the three-dimensional crack face. The reader should note that each pixel being assigned a particular color (black, red, blue, green or white, in order of

increasing opening) is accurately located in space relative to the white contour lines showing sample geometry. For brevity, only the amount of crack opening at the maximum load is shown in Figure 6, although similar plots have been prepared for the minimum load and for the difference in opening between maximum and minimum loads. The arrow in Figure 6 points to a very prominent asperity face which, even at maximum loading, is nearly closed. The resulting mixed I-III mode contact upon unloading may be typical of contact producing maximum closure indications.

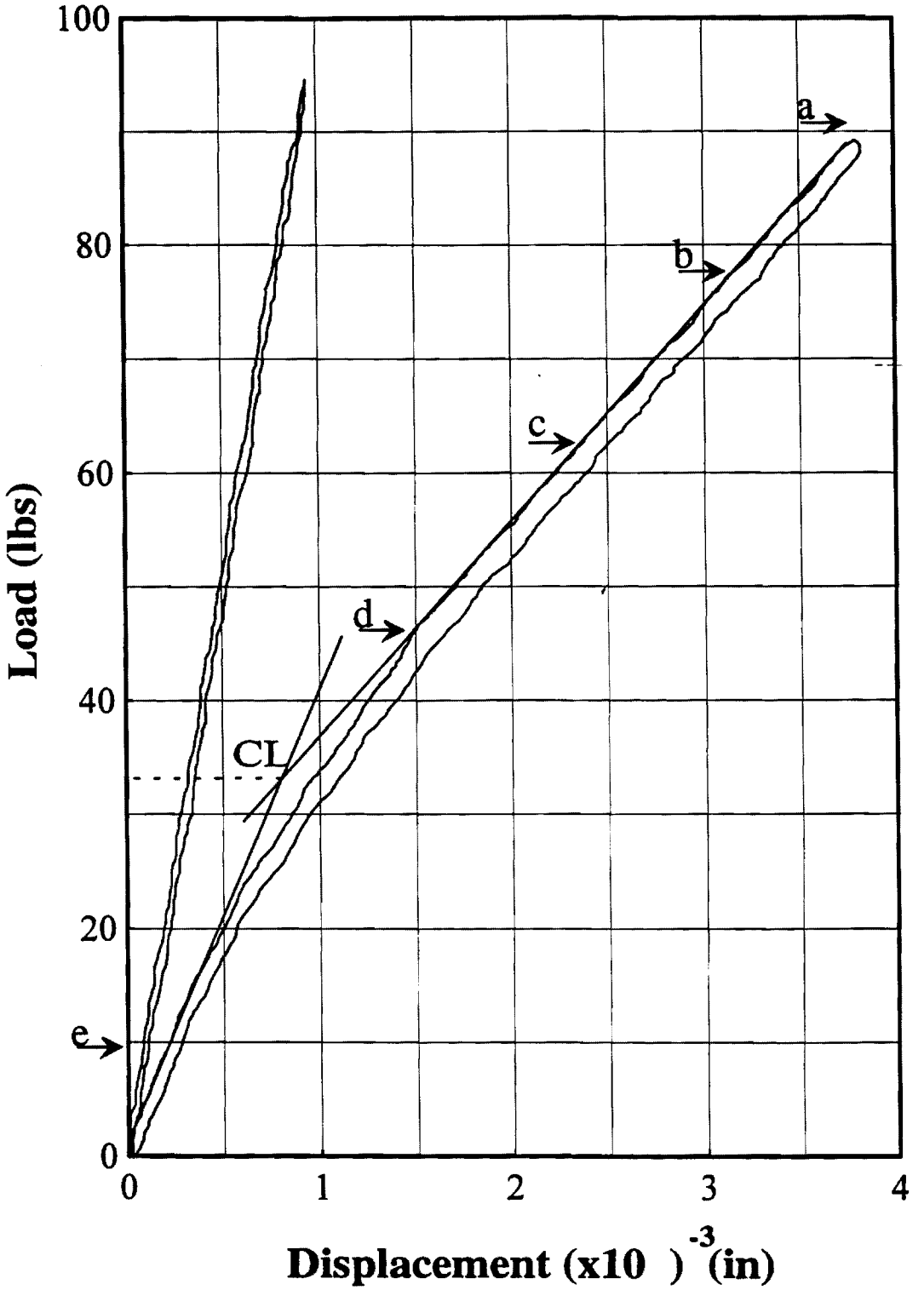

Figure 1. Load-displacement curve for sample CT-2 for the same crack length as for the computed tomography imaging. The letters a-e indicate the loads at which x-ray imaging was carried out, and "CL" indicates the closure load determined by linear extrapolation of the upper and lower portions of the curve.

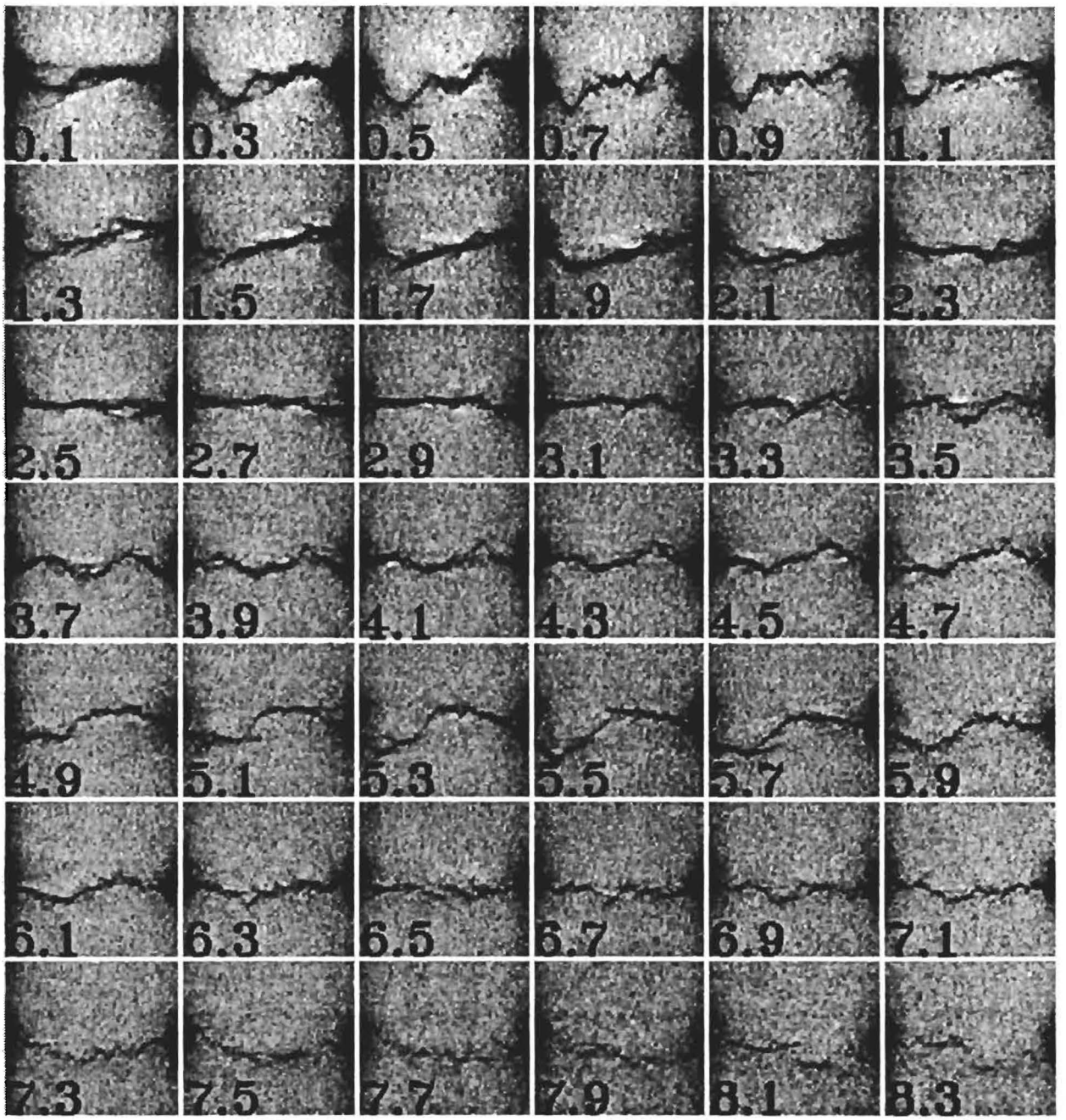

Figure 2. Series of reconstructed sections parallel to the notch tip and showing the crack morphology in sample CT-2. Lower absorption pixels are darker, and the numbers indicate the distance between the cut and the tip of the notch (in mm). The two side-grooves appear on the left and rights sides of each cut, and their separation is 1.75 mm.

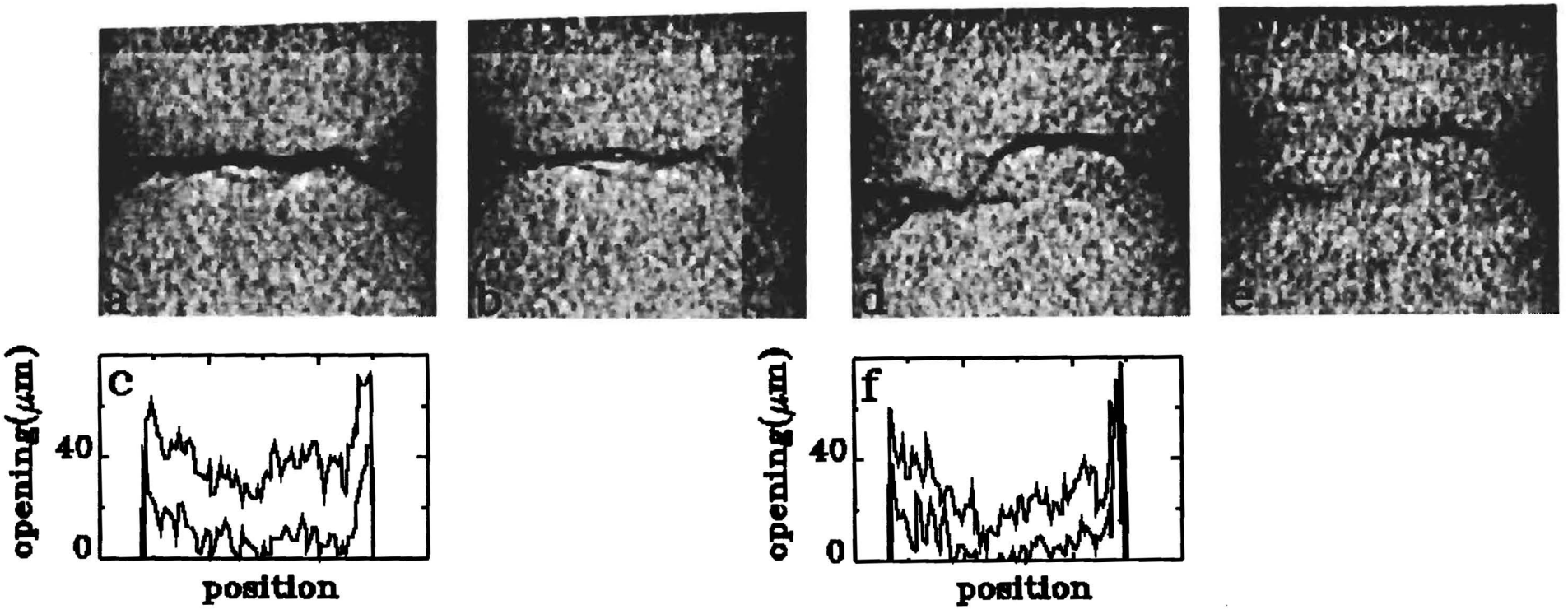

Figure 3. Cuts and measured crack openings. In the images the darker pixels show lower x-ray attenuation, the stress axis is vertical and the ends of the side-grooves, visible at the left and right center of each image, are 1.75 mm apart. a. and b. are cuts 2.96 mm from the end of the notch under 42 kg and 8 kg load, respectively. d. and e. are cuts 5.12 mm from the notch under 42 kg and 8 kg load, respectively. c. and f. show crack opening across each cut 2.96 mm and 5.12 mm from the notch, respectively; the upper curve in each corresponds to the higher load.

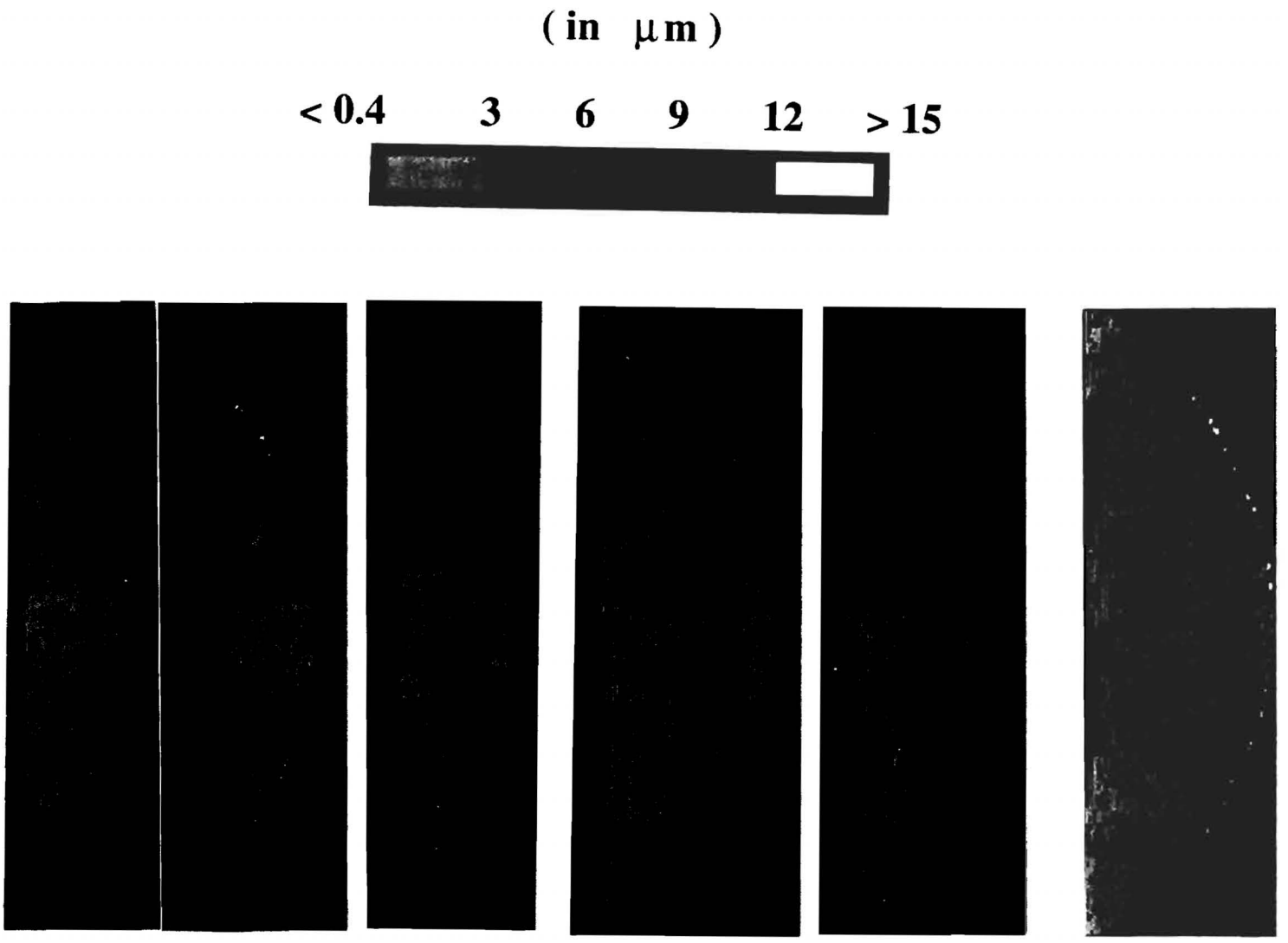

Figure 4 Crack openings measured parallel to the load axis. The color bar indicates the ranges of opening shown for 60, 70, 80, 90 and 100 lbs (22.7, 27.2, 31.8, 36.3, 40.9 and 45.4 kg) loads.

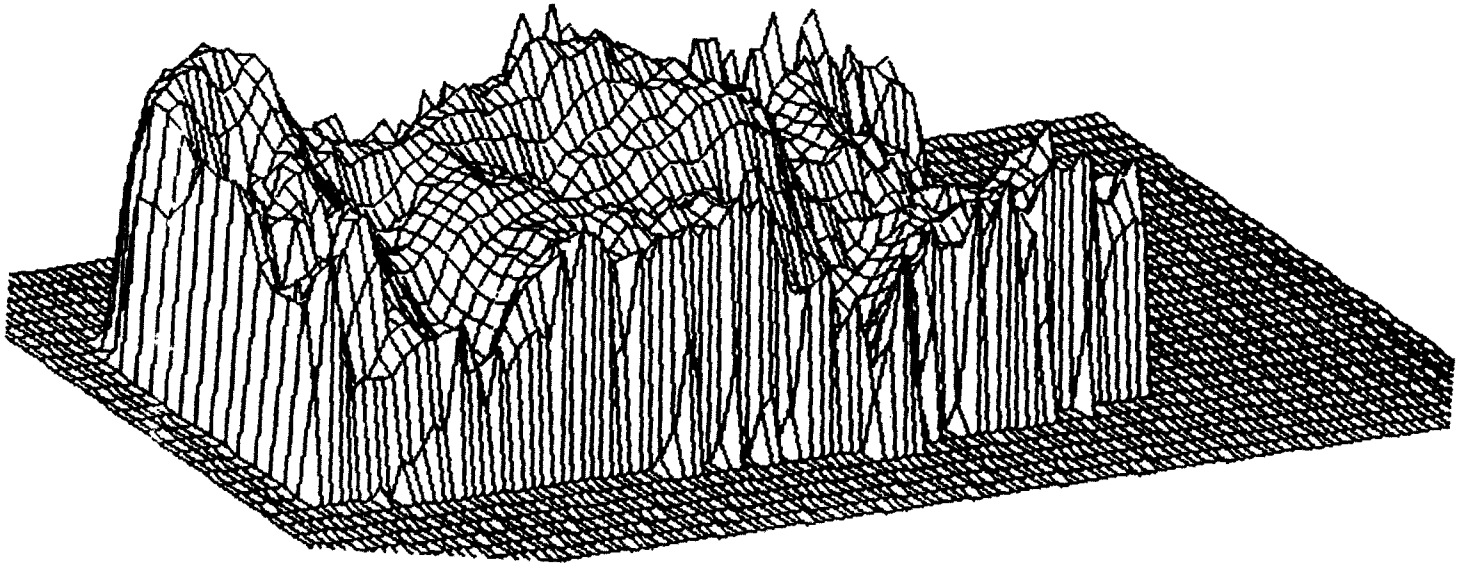

Figure 5. Contour map of crack face position within sample CT-2. The notch is at the left, and the tip of the crack is slightly beyond the right edge of the sample

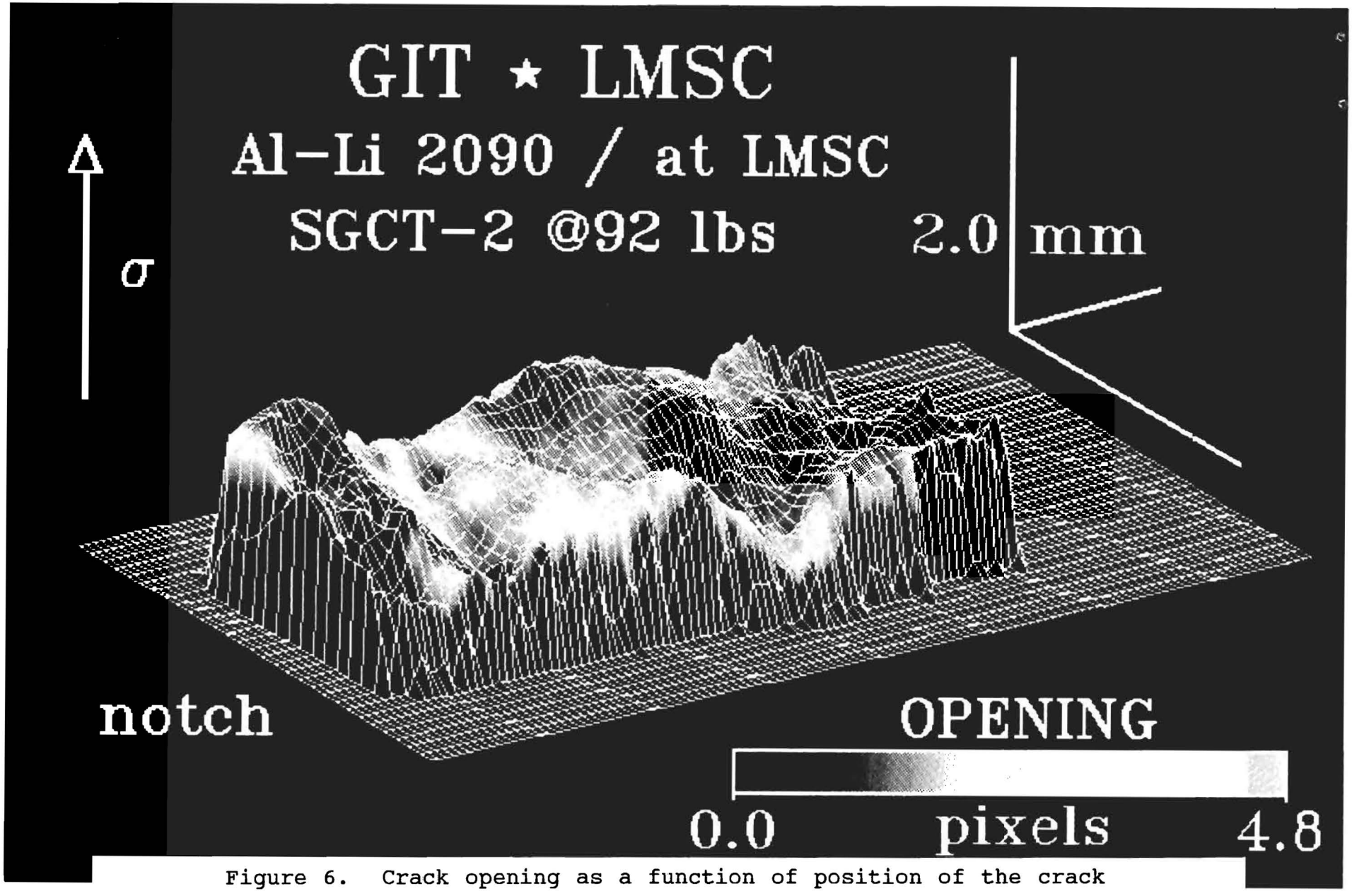

Figure 6. Crack opening as a function of position of the crack faces for the maximum load on sample CT-2. The contour lines delineate position, and the color progression black, red, blue, green and white denotes increasing opening.